IEEE Access
Multidisciplinary | Rapid Review | Open Access Journal

Received 25 November 2022, accepted 17 December 2022, date of publication 23 December 2022,
date of current version 29 December 2022.

Digital Object Identifier 10.1109/ACCESS.2022.3232062

RESEARCH ARTICLE

Improved Deep Learning-Based Energy Management Strategy for Battery-Supercapacitor Hybrid Electric Vehicle With Adaptive Velocity Prediction

CHIGOZIE UZOCHUKWU UDEOGU, (Student Member, IEEE), AND WANSU LIM, (Member, IEEE)
Department of Aeronautics, Mechanical and Electronic Convergence Engineering, Kumoh National Institute of Technology, Gumi-si 39177, South Korea
Corresponding author: Wansu Lim (wansu.lim@kumoh.ac.kr)

This work was supported in part by the Ministry of SMEs and Start-Ups, South Korea, under Grant S3010704; and in part by the National Research Foundation of Korea under Grant 2020R1A4A1017775 and Grant 2021R1I1A3056900.

ABSTRACT The uncertainties and disturbances in the actual driving conditions of hybrid electric vehicles (HEVs) complicate the design of energy management strategy (EMS). To achieve better EMS performance for a battery-supercapacitor HEV, this paper proposes an improved and adaptive deep learning-based velocity prediction control EMS that can prolong the battery lifetime through efficient utilization of both the battery and supercapacitor. First, feature engineering techniques are used to extract and increase the key features from the historical driving cycle data of known driving conditions. With the extracted features, an improved long short-term memory (LSTM) velocity predictor was developed to predict future driving cycles for a real-time EMS under an unknown driving condition. Second, a real-time EMS based on the rule-based framework optimized with a neural network is proposed to optimize the power allocation online. Simulation results show that the proposed strategy smoothens battery peak power (i.e. prolongs battery life span) by approximately 26.85% on average and increases supercapacitor participation in the EMS, as evidenced by its increased energy throughput. Furthermore, compared with other EMS approaches, the proposed strategy improved the efficiency by significantly reducing total energy losses by approximately 22.25%. These results validate the reliability and robustness of the proposed strategy.

INDEX TERMS Battery, deep learning, drive cycle, electric vehicle, energy management, feature engineering, k-medoids, rule-based, supercapacitor.

I. INTRODUCTION

Electric vehicles (EVs) have proven to be a sustainable and efficient solution to the rising global environmental issues related to gas emissions [1]. Generally, batteries are used as the main energy source in EVs because of their high energy density property and ability to store most of the onboard electrical energy. However, batteries have low power density, hence cannot meet the peak power demand of EVs under climbing conditions or acceleration. This shows dynamics of batteries necessitate the use of auxiliary energy sources, such as supercapacitors (SCs). Thus, hybrid electric vehicles (HEV), which combine batteries and SCs have been studied in recent years. SCs have high power density but low energy density hence these contrasting properties of battery and SC make them good complements [2]. The SC and battery hybrid energy storage system (HESS) of HEVs is such that combines the merits of both the battery and SC. It utilizes the high energy density of the battery to supply energy to the vehicle over a driving mission and the high power density of the SC to satisfy a gap of peak power demand during transients and regenerative braking of the vehicle [3], [4]. As such,

The associate editor coordinating the review of this manuscript and approving it for publication was Guijun Li.

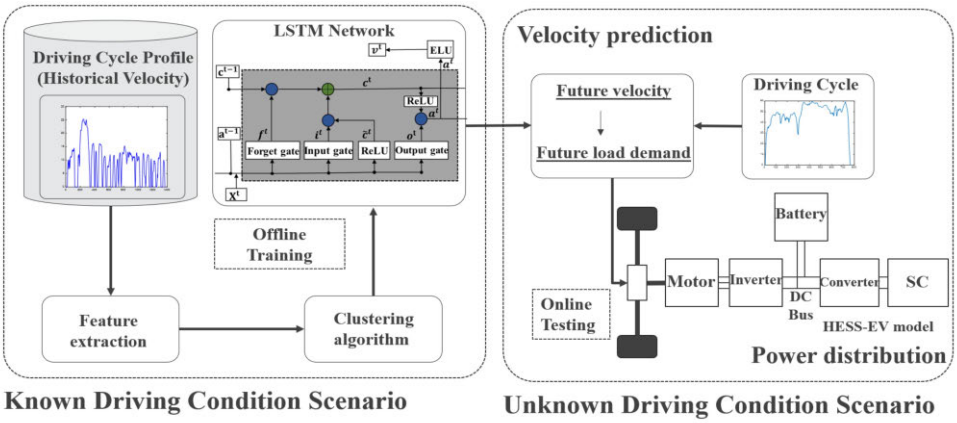

FIGURE 1. System configuration.

the SC can handle high power peaks and elongate battery lifetime [5].

Energy management is a critical technology in HEV, which can determine the optimal power split control for the energy source subsystems. Generally, the existing energy management strategies (EMSs) of HEVs are grouped into heuristic and optimization-based strategies [6], [7]. The heuristic strategies include the rule-based [8] and the fuzzy logic-based [9] while the optimization-based strategies include dynamic programming (DP) [10]. [8] proposed a rule-based EMS for the HESS based on the adequate discharge of the SC pack to ensure the utilization of all available energy from the regeneration mode, hence improving EV performance and range. [9] proposed an EMS for a HESS in EV based on fuzzy logic which elongates the battery lifetime by considering the state of charge (SOC) of the SC, power demand, and speed of the EV. [10] utilized a DP-based optimal control algorithm to formulate an EMS for a plug-in HEV which conquered the numerical problems associated with the accuracy and computational burden of DP.

There are other popularly used algorithms for EM control strategies of HEVs. Some of these include Pontryagin's minimum principle (PMP) [11], [12], model predictive control (MPC) [13], equivalent consumption minimization strategy (ECMS) [14], [15], robust control [16], slope-weighted energy-based rapid control analysis (SERCA) [17], frequency-based [18], wavelet-based [19], hybrid approach [20] and so on. Varying degrees of improvement are realized using these schemes in hundreds of literature. Amongst all the optimization-based strategies, DP is the only algorithm broadly recognized to possibly guarantee theoretical optimal control results [21]. However, it operates with the assumption that the entire drive cycle and power demand profile are known and hence cannot provide real-time or online applications. This is because real-life driving situations always have degrees of uncertainty and disturbance of actual conditions [22]. Thus, an EMS that can capture the degree of future driving uncertainties is needed.

With the rapid development of artificial intelligence technologies, machine learning-based methods are increasingly applied to EMS [23]. They have been used in combination with some of the optimization-based strategies to achieve real-time application of optimal EMS control [24], [25], [26], [27]. However, these results are achieved on the basis of a degree of certainty and known driving conditions. Since the uncertainty and disturbance of actual conditions hugely increase the difficulty of EMS design of HEVs, it is important to develop an efficient and adaptive EMS that can achieve real-time application in unknown driving conditions. Adaptive and real-time applications of the formulated EMSs in complicated unknown future driving situations are still the struggling direction since the existing techniques are based on known driving situations. Future driving information is a prerequisite for an adaptive EMS [28]. The more realistic the forecasting driving information provided for the EMS is, the more likely it is to make an appropriate decision for the power split between the component energy sources even in an unknown driving situation. The driving cycle is a random time-series data and machine learning can be exploited to deal with enormous driving data. Therefore, to adaptively control the power split of the HEV energy sources for real-time applications in unknown driving scenarios, we propose an improved deep learning-based energy management strategy for battery-SC HEV with an adaptive velocity prediction utilizing the long short-term memory (LSTM) model to predict future driving velocity of an unknown driving scenario. LSTM is a deep learning model, well-known for its strong abilities in handling and forecasting time series data made possible by its unique ability in learning and remembering historical information. It is also well-suited to be trained to learn a highly nonlinear input/output relationship. Since velocity prediction is a nonlinear problem with high dynamics, LSTM is a suitable solution and is then utilized. Hence, the expectation is that designing an EMS based on velocity prediction will lead to load demand prediction for the energy source subsystems of the HESS which is

essential in prolonging the lifetime of the component energy systems.

The contributions of this paper are as follows:

1) To address the challenge of uncertainties and disturbances of actual driving even in unknown driving conditions, the paper proposes an adaptive LSTM-based velocity prediction EMS for HEVs that considers and handles the future uncertainties of real-life driving conditions to improve mobility and extend battery life.

2) To enhance velocity prediction accuracy, an improved time-series LSTM model with feature engineering prediction scheme is implemented.

3) To ensure better EMS performance and achieve enhanced efficiency, a new approach to split the power between the battery and SC in such a way that both battery and SC SOCs drain at an overall similar rate is proposed. This is also geared towards better utilization of both energy storage devices.

The rest of the paper is organized as follows: The system architecture and HEV modeling are presented in Section II. Section III describes the velocity prediction implementation. The design of the energy management strategy and simulation results analysis is presented in Section IV and V, respectively. Section VI summarizes and concludes the paper.

II. SYSTEM CONFIGURATION AND HEV MODELING

Figure 1 shows the overall system configuration of the proposed EMS model. It is composed of the velocity prediction part and the power distribution part. During the velocity prediction, the LSTM model is used to predict the velocity of the vehicle. Historical driving cycle profile dataset from known driving conditions is used to train the LSTM model offline. The trained LSTM model is then used to predict future velocities of unknown driving condition scenarios in the online testing stage. With the predicted future velocities, the vehicle system generates the corresponding power demand by extension. The system's power distribution part is responsible for accurately splitting the future power demand among the onboard energy sources in the HESS i.e., battery and SC. The dual converter topology was adopted for the onboard energy sources following research [29]. The battery and SC are connected to the system through their dc-dc converters, as shown in Fig. 2, using the component data given in Table 1. Both the battery and SC are actively controlled through their individual dc-dc converters. Interlinking the individual energy source controller with the motor drive through an inverter is the dc-link. The dc-link acts as the power bus of the system. The battery and SC powers can be controlled by tuning the duty cycles of their dc-dc converters.

The building blocks of the vehicle model for establishing the power flow are given in [30] and ADVISOR [31] as shown in Fig. 3. As seen in the figure, the vehicle wheels and axles which are connected to a one-stage gearbox through the final drive is driven by the motor. There are two stages of the power flow, that is, backward- and forward-facing approaches. The backward-facing approach determines the power required by each building block of the vehicle based on the driving cycle. However, the forward-facing approach takes the overall power input from the backward-facing approach as the power that the battery and SC should contribute, while meeting each building block constraint. The regenerative braking mode of the vehicle occurs when power flows from the wheels of the vehicle to the onboard energy sources, hence it is denoted

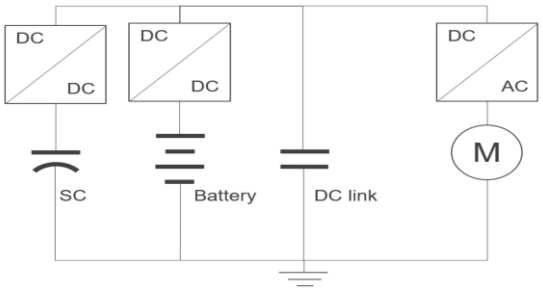

FIGURE 2. EV dual converter topology.

TABLE 1. Components of the dc-dc converter.

Item	Specifications
DC Bus Electrolytic Capacitor	2x15mF, 200V capacitors in parallel
Battery Electrolytic Smoothing Capacitor	4700μF, 200V
Supercapacitor Electrolytic Smoothing Capacitor	4700μF, 200V
Switches	600V, 300A IGBTs
Battery Inductor	180μH, 300A air core inductor
Supercapacitor Inductor	300μH, 300A air core inductor

TABLE 2. Components of the dc-dc converter.

Parameter	Value	Parameter	Value
Battery Type	Li-ion	Cells in Module	3 in series
Battery Cell	6 Ah/3.9V	Battery Modules	31 in series
Battery Cell	0.378 kg	Battery Pack	6 Ah/362.7V
SC Type	PC2500	SC Cells	120
SC Voltage	2.5V	SC Cell	0.71 kg
SC Current	± 225A		
BEV Mass	830 kg	$C_{rolling}$	0.012
Frontal Area	2.03 m^2	$C_{Air-drag}$	0.19
Motor Type	IM (AC75)	Motor Torque Scale	0.268
Motor Power	20 kW	Initial Temp.	30 ºC
Cargo	136 kg		

TABLE 3. Vehicle model files.

File Name	File Name
MC AC75	ACC HYBRID
VEH SMCAR	ESS2 LI7 tmp
ESS SC2 Maxwell	EV dual in
WH SMCAR	init conds
TX 1SPD	gui run files
PTC EV	recompute mass

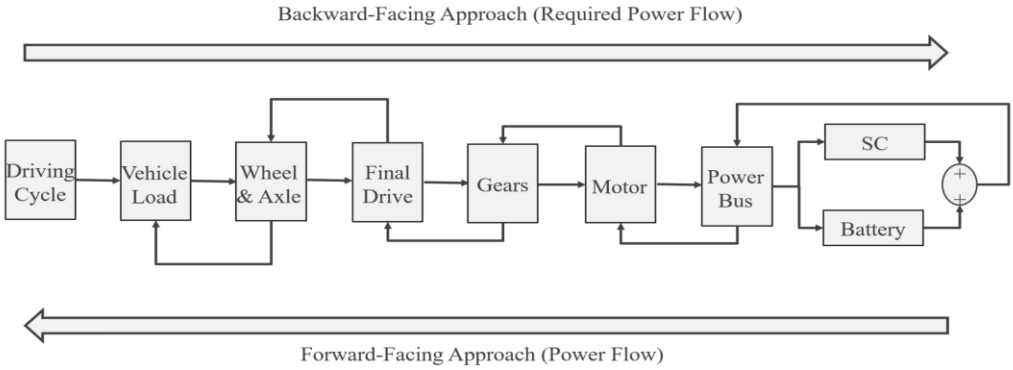

FIGURE 3. Building blocks of battery-SC vehicle model [30], [31].

with a negative power convention in this paper. Similarly, the propulsion (driving) mode occurs when power flows from the onboard energy sources of the vehicle to the wheels, thus a positive power convention. The vehicle parameters and model files used in this paper are according to [32] and given in Tables 2 and 3.

III. VELOCITY PREDICTION BASED ON LSTM NETWORK

In this section, the dataset and feature engineering techniques used are described. Furthermore, single and multiple time-series velocity prediction methods using the LSTM network are discussed.

A. DATASET AND FEATURE ENGINEERING

To predict velocity, information like historical driving data, weather, traffic, and road information is needed [33]. Since this information is difficult to obtain, in this paper, typical driving cycles are adopted. The driving cycle is a vehicle velocity profile with random, time-varying uncertainties. The drive cycle prediction can be treated as a non-linear time series prediction with high dynamics. Hence, LSTM is utilized due to its capacity in dealing with such problems. LSTM has proven strong abilities in handling and forecasting time series data due to its unique ability in learning and remembering historical information. It is also well-suited to be trained to learn a highly nonlinear input/output relationship [34], [35], [36].

Eight different standard driving cycle datasets were obtained and combined to form a known driving condition scenario using the Driving Cycle Simulink Block in MATLAB. The obtained combined driving cycle dataset was used to train the LSTM model. The eight driving cycles include NYCC, REP05, US06, WVUINTER, NEDC, WVUCITY, US06_HWY, and WVUSUB. The velocity profile of the training driving cycle dataset is shown in Fig. 4. For testing the network, three different sets of standard driving cycle datasets were obtained to depict an unknown driving condition scenario as the network does not know these driving cycles nor was it trained with them. The three driving cycles include UDDS, SC03, and HWFET. The criteria for selecting

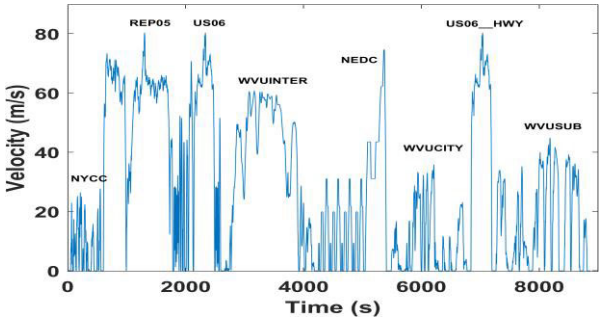

FIGURE 4. Sample training driving cycle dataset.

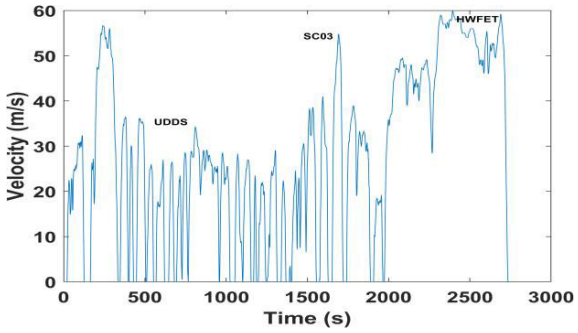

(a)

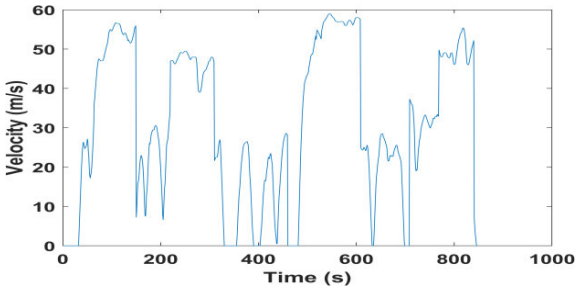

(b)

FIGURE 5. (a) Non-randomized testing driving cycle combination. (b) Randomized testing driving cycle.

these three driving cycles are based on: 1) They should come from real vehicle testing to reflect real-life driving conditions. 2) They should be standard driving cycles that are

popularly used. 3) They should be typical of three kinds of driving scenarios: urban (UDDS), suburban (SC03), and highway (HWFET) [37]. To further test the adaptability of the model to predict future velocities, especially in unknown driving scenarios, a new driving cycle dataset called randomized driving cycle was created. The randomized driving cycle was created with data points obtained by moving randomly and interchangeably from the UDDS to SC03 to HWFET driving cycles. Thus, two sets of testing drive cycles were evaluated: non-randomized (i.e. UDDS, SC03, and HWFET) and randomized. Figure 5 shows the velocity profile of the testing driving cycle dataset.

Feature engineering involves the transformation of data into features that state the problem of the predictive model well to improve model performance and reduce complexity [38]. The driving cycle dataset has only one feature of velocity, v, this hampers the prediction performance of the LSTM model as many input features can improve its accuracy. To cope with this challenge, feature engineering was conducted on the dataset to obtain more features that represent the dynamic operating nature of vehicles in diverse driving conditions. The steps of the feature engineering process are outlined as follows:

1) The dataset is divided into segments of 60 seconds each.

2) Corresponding average velocity and average acceleration are calculated for each segment.

3) Using the velocity profile, the acceleration/deceleration profile is obtained.

4) Utilizing the obtained acceleration/deceleration profile, uniform velocity and maximum velocity are obtained.

Hence, for each segment, five features (three velocity and two acceleration) each are obtained i.e., Velocity features: average velocity v_{avg}, uniform velocity v_{unif} and maximum velocity v_{max}; Acceleration features: average acceleration a_{avg}, and instant acceleration, a. Therefore, each time instant $[v]$ of the original dataset is transformed into $[v, v_{avg}, v_{unif}, v_{max}, a_{avg}, a]$. Next, the features are clustered into different driving conditions using the k-medoids clustering algorithm. Here, k-medoids is chosen due to its ability to effectively deal with noise and outliers in data [39]. The k-medoids algorithm flowchart is shown in Fig. 6. The algorithm can be explained as follows:

1) Randomly choose k objects from N objects in data and assign k objects to k medoids, each medoid represents a cluster. 2) For all remaining non-medoid objects, compute the distance from all medoids, then assign non-medoid objects to clusters according to the similarity measure.

3) Re-calculate k medoids according to similarity measure, if within the error limits for the termination criterion, terminate the algorithm. If the conditions are not met, return to step 2.

Finally, the driving conditions are classified into three conditions describing real-world driving conditions namely urban, suburban, and highway denoted by one, two, and three, respectively.

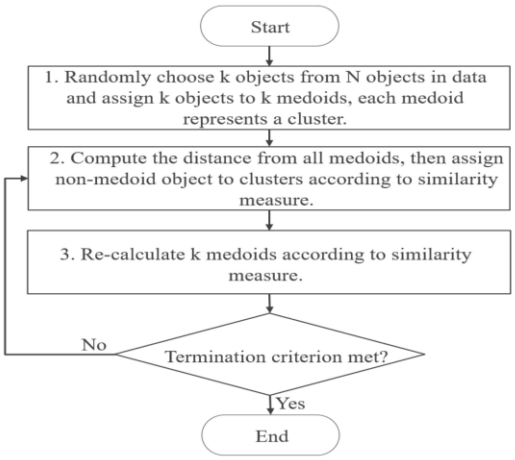

FIGURE 6. Flowchart of k-medoids algorithm.

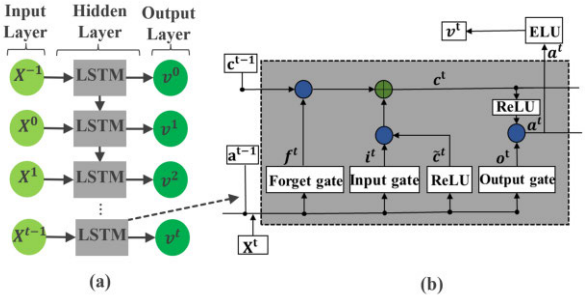

FIGURE 7. (a) Overall diagram of LSTM network. (b) Structure of LSTM cell.

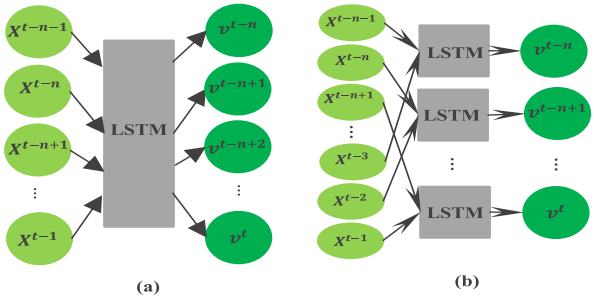

FIGURE 8. Framework of LSTM (a) single time-series scheme (b) multiple time-series scheme.

B. VELOCITY PREDICTION USING LSTM

The LSTM network is designed to learn long-term dependencies. It remembers information for long periods of time, can discard redundant information and selects key information to be stored in the internal state. It controls the flow of information throughout its network via its three gates namely the input gate i^t, forget gate f^t and output gate o^t. The overall diagram of LSTM network is shown in Fig. 7 (a) and Fig. 7 (b) is an illustration of a single LSTM cell. The $\tilde{c}^t$ is the candidate cell status, the c^t is the new cell status and the LSTM cell hidden state a^t transfers signals to the next cell.

TABLE 4. Results of the time-series schemes.

Scheme	Driving Cycle							
	UDDS		SC03		HWFET		Randomized Cycle	
	MAE (%)	RMSE (%)	MAE (%)	RMSE (%)	MAE (%)	RMSE (%)	MAE (%)	RMSE (%)
Single time-series (without feature engineering)	1.005	1.450	0.980	1.555	0.520	0.755	1.093	3.440
Single time-series (with feature engineering)	0.224	0.256	0.207	0.242	0.237	0.276	0.301	0.424
Multiple time-series (with feature engineering)	**0.121**	**0.131**	**0.048**	**0.055**	**0.126**	**0.142**	**0.141**	**0.213**

The mathematical representations of the different weights and gates of the LSTM cell are [40]:

$$i^t = \sigma(W_i \left[a^{(t-1)}, X^t\right] + b_i) \quad (1)$$

$$f^t = \sigma(W_f \left[a^{(t-1)}, X^t\right] + b_f) \quad (2)$$

$$\tilde{c}^t = \varphi(W_c \left[a^{(t-1)}, X^t\right] + b_c) \quad (3)$$

$$c^t = f^t * c^{t-1} + i^t * \tilde{c}^t \quad (4)$$

$$o^t = \sigma(W_o \left[a^{(t-1)}, X^t\right] + b_o) \quad (5)$$

$$a^t = o^t * \varphi(c^t) \quad (6)$$

where, $\tilde{c}^t$ is candidate to update c^t, φ is ReLU, i^t is input gate, f^t is forget gate, o^t is output gate, and $W_\blacksquare$ is weights for different activations, $\blacksquare \in \{c, i, f, o;$ *c and i are input, f is forget, o is output*$\}$.

The LSTM network is used in predicting the future velocity of the HEV. The velocity, acceleration, and type of driving situation at any given time, as obtained from the feature engineering process described earlier, served as input, X^t, of the LSTM network i.e. $X^t = [v^t, a^t, d^t]$, where v^t, a^t, d^t are velocity, acceleration, and type of driving situation at time, t, respectively. By brute-force search, the structure of the LSTM is set to have one hidden layer with 50 cells. To improve the prediction accuracy of the model, single and multiple time-series prediction schemes were carried out with the input features. The framework of the single time-series scheme is shown in Fig. 8(a). For n number of inputs, each input feature passes through all the cells of the LSTM. For the multiple time-series scheme, the input features are divided into subgroups, n. Each subgroup input feature targets one output at any time instant, as illustrated in Fig. 8(b).

C. COMPARISON OF THE TIME-SERIES PREDICTION SCHEMES

To evaluate the performance of the model in predicting future velocity, the single time-series prediction with and without feature engineering results (i.e. original dataset) and the multiple time-series prediction with feature engineering results are compared. The evaluation is based on the mean absolute error (MAE) and root mean square error (RMSE). Generally, the lower these values, the higher the prediction accuracy.

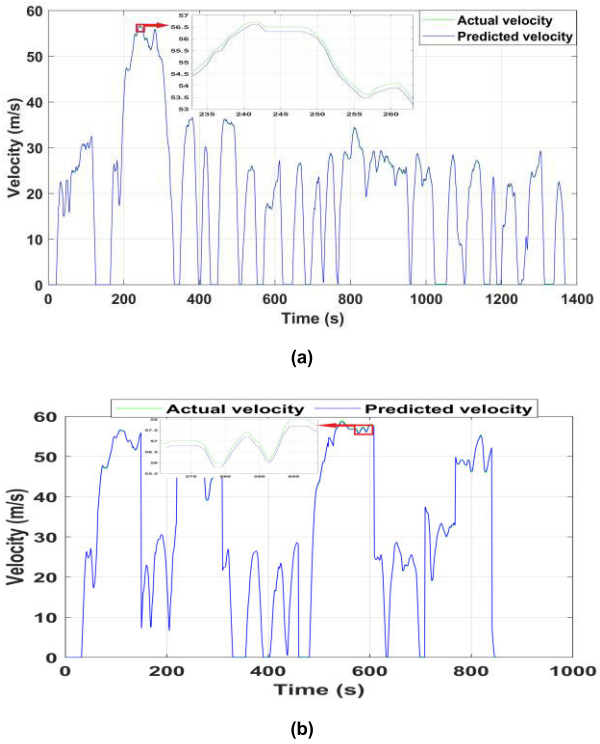

FIGURE 9. Velocity prediction results of the multiple time-series (with feature engineering) scheme for (a) UDDS, (b) Randomized driving cycles.

1) NON-RANDOMIZED DRIVING CYCLE

The results of the velocity prediction of the UDDS, SC03, and HWFET driving cycles are displayed in Table 4 with the prediction result plot of the UDDS shown in Fig. 9 (a). As shown in Table 4, for the UDDS, the single time-series prediction without feature engineering results had MAE and RMSE values of 1.005 and 1.450 respectively while the single time-series prediction with feature engineering results had MAE and RMSE values of 0.224 and 0.256 respectively. This represents a 77.71% and 82.34% improvement in the MAE and RMSE values of the two single time-series prediction schemes, respectively. Similar results were seen with the SC03 and HWFET datasets. This illustrates the improvement capabilities of the feature engineering technique on the velocity prediction process. Furthermore, the multiple time-series

prediction (with feature engineering) scheme for the UDDS had MAE and RMSE values of 0.121 and 0.131 respectively. The results when compared with the single time-series (with feature engineering) scheme showed a further improvement of the prediction accuracy by 45.98% and 48.38% in MAE and RMSE, respectively. As shown, the multiple time-series prediction (with feature engineering) scheme had the best results on all three non-randomized driving cycle datasets. Hence, it is an improved time-series method for velocity prediction using LSTM.

2) RANDOMIZED DRIVING CYCLE

The randomized driving cycle, which represents a further higher level of uncertainty and disturbance while driving in an unknown driving scenario, is also tested to see how well the model responds in predicting the velocity. The results as shown in Fig. 9 (b) and Table 4 indicate similar outcomes with the non-randomized cycles. The single time-series (with feature engineering) scheme enhanced the results of the single time-series (without feature engineering) by 72.46% and 87.67% in the MAE and RMSE values, respectively. With MAE and RMSE values of 0.141 and 0.213, respectively, the multiple time-series (with feature engineering) scheme exhibited further improvement when compared with the results of the single time-series (with feature engineering) scheme. To be precise, it improved by 53.16% and 49.76% in MAE and RMSE, respectively. This implies that the LSTM model having effectively learned the driving conditions of the known scenarios in the offline stage, when deployed online, had adaptively adjusted and was capable of successfully handling the uncertainties encountered in the unknown driving conditions, thus predicting future velocity more accurately. Additionally, the results further validate the multiple time-series (with feature engineering) scheme as the best-improved LSTM velocity prediction scheme among the three schemes. Moreover, the real-time velocity prediction of the single time series took 0.337 ms, while that of the multiple time series took 0.975 ms. Although the multiple time series scheme consumes more computational burden, it takes less than 1 s. This processing time accords with the requirement for real-time energy management, hence it can give the prediction within the instant control time step and can be implemented in real-time. Therefore, this scheme was adopted for predicting future velocities in this paper.

IV. POWER DISTRIBUTION SCHEME

In this section, a decentralized control scheme to distribute power for the HESS based on a rule-based framework is developed. The objectives of the framework are geared towards better utilization of both battery and SC while achieving enhanced efficiency. It intends to manage the state of charge (SOC) of the SC by ensuring its availability all through the battery discharge period. Hence, the control philosophy of the proposed approach is to manage and regulate the SC discharge rate based on the knowledge of the vehicle velocity, the current status of the SC, and the battery SOC. To achieve these objectives, the following principles are adhered to: 1) SC participates during regenerative braking. 2) Battery does not charge SC but only supports the load. 3) Both the battery and SC participate during acceleration. With these concepts, an original rule-based control strategy is developed. However, in order to achieve the proposed power distribution scheme, a neural network-based approach is developed and

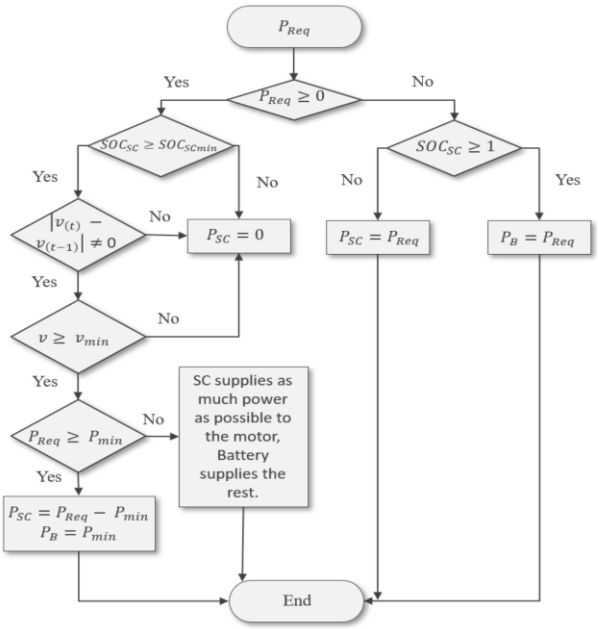

FIGURE 10. Flowchart of the original rule-based energy management strategy.

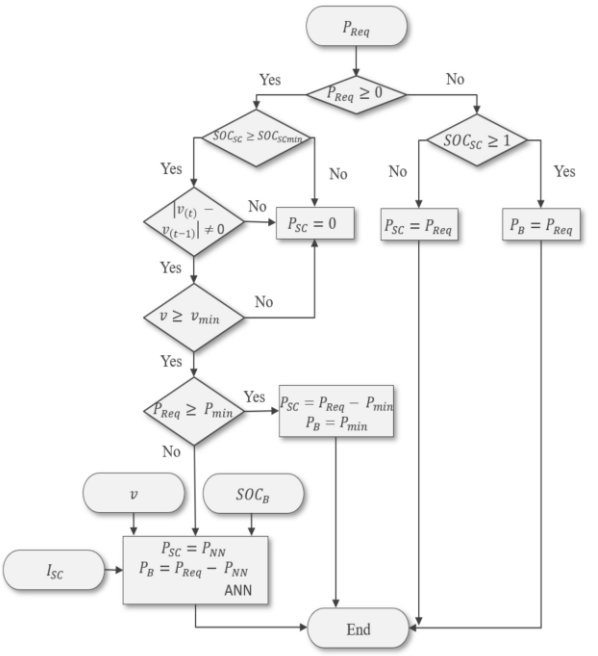

FIGURE 11. Flowchart of the proposed energy management strategy.

integrated into the rules to achieve enhanced efficiency. The original rule-based energy management (i.e., power distribution) strategy and the proposed neural network-based scheme are explained in the following subsections.

A. ORIGINAL RULE-BASED ENERGY MANAGEMENT STRATEGY

In this scheme, the SC only get to contribute to the vehicle propulsion stage when its SOC is above a certain minimum value and the vehicle is accelerating or decelerating at a certain speed. Once the required conditions are met, the SC participates in the power-sharing as the remaining power is handled by the battery. The flowchart of the original rule-based control strategy is shown in Fig. 10. At first, the power required by the vehicle, P_{Req}, is calculated. If P_{Req} is below zero (i.e., negative), it implies regenerative braking mode. The state of the SC, SOC_{SC}, is evaluated, and based on its level it is either charged or not. If P_{Req} is above zero (i.e., positive), it implies propulsion (driving) mode hence the vehicle needs energy to move. The SOC_{SC} is evaluated again but this time against its minimum threshold, SOC_{SCmin}. If below the value, the battery alone supplies all the power requirements of the vehicle as the SC cannot support below its minimum threshold. This minimum threshold value is determined based on the minimum voltage required by the motor drive as modeled in ADVISOR. If the SOC_{SC} is above its minimum threshold, then the vehicle dynamics is analyzed. Based on the present and previous velocities of the vehicle, it can be computed if the vehicle is accelerating or decelerating or at a constant velocity. The SC supports only when there is a change in velocity (i.e., acceleration or deceleration). If the vehicle is established to be accelerating/decelerating, the SC will only support if the vehicle velocity, v, is greater than v_{min}. v_{min} is established by finding a velocity at which regeneration power is zero during braking as simulated by ADVISOR. Next, to elongate the battery lifetime and ensure better utilization of the battery and SC during the power distribution, a P_{min} value is established. P_{min} is set to be the peak power requirement of the vehicle during regenerative braking. The idea here is that a vehicle experiences several accelerations and deceleration/regenerative braking events according to its driving cycle. Hence, for every acceleration, there will be a certain deceleration/regenerative braking at some point during the cycle thus this provides information to the HESS on the amount of energy that could be required during propulsion. If the P_{Req} is greater than this value, then the battery supplies the P_{min} while the SC supplies the remaining. But if P_{Req} is less than the P_{min}, then the SC supports with as much power as possible as it can to the motor while the battery supplies the rest. Thus, at any given instance, the power distribution between the battery and SC is represented mathematically as:

$$P_{Req} = P_B + P_{SC} \tag{7}$$

where P_{Req} denotes power requirement of the motor of the vehicle, P_B denotes battery power and P_{SC} denotes SC power.

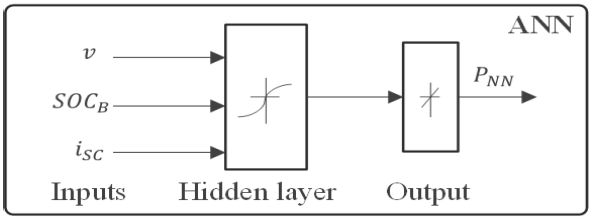

FIGURE 12. Architecture of the ANN.

B. OVERALL PROPOSED ENERGY MANAGEMENT STRATEGY

To reduce energy loss, achieve enhanced efficiency, and better utilization of the battery and SC during the power-sharing stage of the original rule-based EMS explained earlier in the previous section, an artificial neural network (ANN) -based approach is designed and incorporated into the rules. ANN has been broadly used for optimal parameter estimation as it is capable of producing the desired results once trained offline and its hidden layer weights are fine-tuned. It can then be deployed in real-time to yield the desired output [41]. The original rule-based EMS is adjusted and updated, as shown in Fig. 11. The ANN introduces intelligence to the power-sharing during the period when $P_{Req} \leq P_{min}$. Its decision is made upon consideration of the vehicle velocity, v, current status of the SC, i_{SC}, and battery SOC, SOC_B, at such periods. This will ensure better participation of both the battery and SC based on their states during this period as against what is obtained in the original rule-based EMS. The architecture of the ANN is shown in Fig. 12. The purpose of the ANN is to determine how much power the SC is expected to contribute during power-sharing with the vehicle velocity, v, current status of the SC, i_{SC}, and battery SOC, SOC_B as inputs. The output of the ANN, P_{NN}, is the power the SC is expected to contribute during the power-sharing, while the battery supplies the remaining. The simulation was carried out in MATLAB/Simulink using the ANN toolbox. The Levenberg-Marquart training algorithm was used to train the ANN as it is known for its fast convergence and robustness. Data points from the 3 driving cycles – UDDS, SC03, and HWFET are used in training the ANN to obtain optimal parameters that will yield optimal P_{SC} and P_B when P_{Req} is less than P_{min}. Furthermore, to achieve the goal of ensuring that both battery and SC deplete approximately at a similar rate, a depletion factor is used during the training process for each driving cycle.

V. EMS VALIDATION AND RESULTS ANALYSIS

This section presents brief explanations of the model simulation and the results of the EMS.

A. SIMULATION OF THE ESS AND HESS MODELS

As shown in Fig. 3, both the single ESS (battery only) and HESS (battery and SC) vehicle models were implemented in ADVISOR. According to [30] and [31], some of the

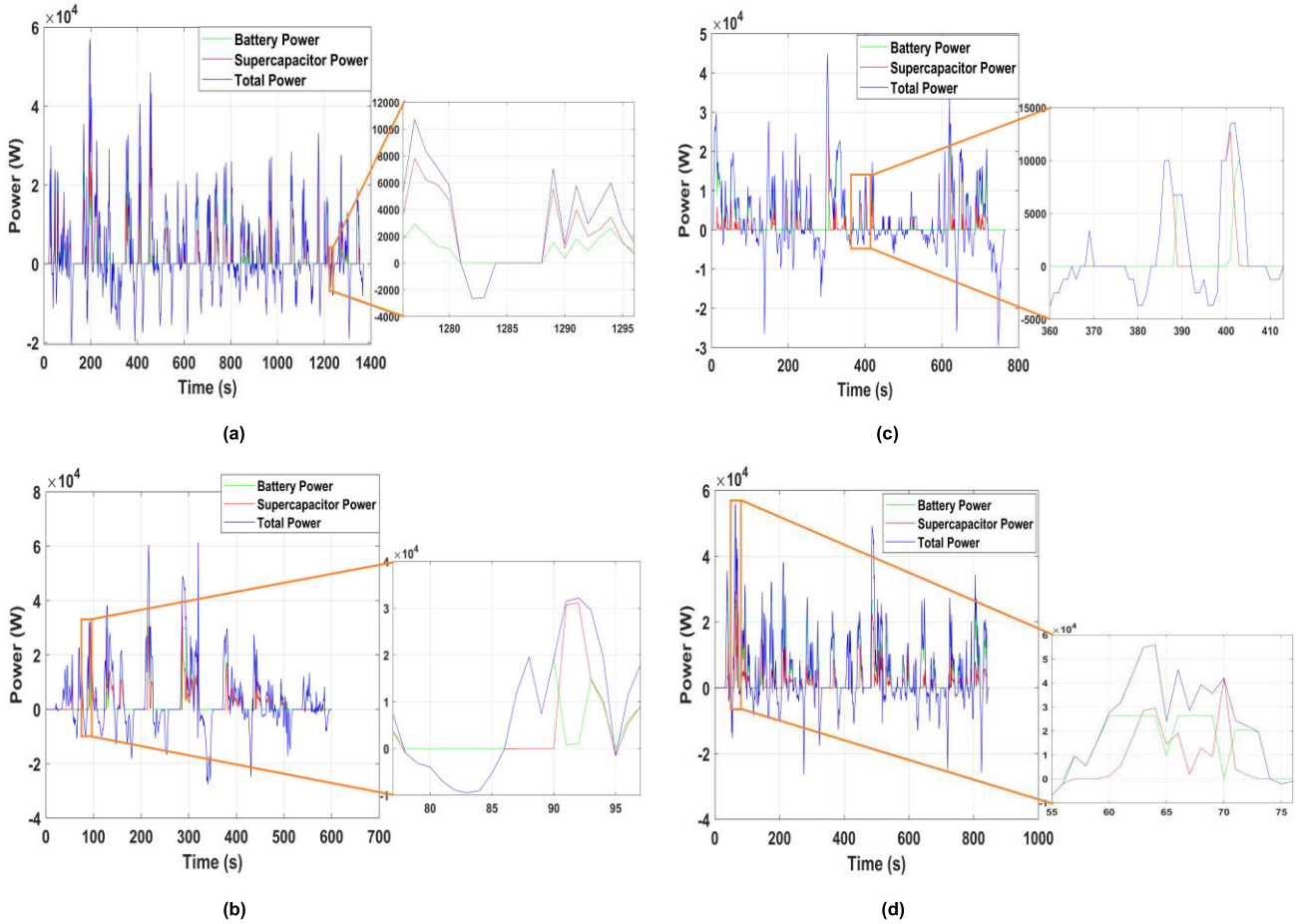

FIGURE 13. Power allocation results of the proposed EMS on (a) UDDS, (b) SC03, (c) HWFET, and (d) Randomized driving cycles.

variables associated with both the battery and SC models include internal resistance, R_{int}, open circuit voltage, OCV, temperature, T, maximum capacity, C_n, and coulombic efficiency, η. For the battery model, η and C_n are mapped according to battery temperature, T_B variation, OCV, and R_{int} are mapped with SOC_B and T_B while R_{int} has a different mapping model for charge R_{ch} and discharge R_{dch}. Similar mapping is used for the SC model utilizing its corresponding parameters. The capacity of SC, compared to battery capacity C_n, is related to the SC capacitance. However, the OCV of SC follows an exponential relationship with SOC_{SC} in accordance with the specified minimum and maximum voltage levels. The model files and parameters used in modeling the single ESS and HESS vehicle models are shown in Tables 2 and 3.

B. PERFORMANCE OF PROPOSED EMS

The minimum and maximum SOC levels of the vehicle battery are 10% and 100%, respectively, while that of the SC are 40% and 98%, respectively. This is to satisfy the inverter-motor minimum operational voltage level requirement as modeled in ADVISOR.

1) NON-RANDOMIZED DRIVING CYCLE

The regenerative braking peak power requirement of the vehicle, which is set as P_{min} value, for the 3 non-randomized driving cycles used in this paper – UDDS, SC03, and HWFET are 20.5 kW, 27.6 kW, and 29.5 kW, respectively, while the v_{min} values are 20.8 m/s, 22.5 m/s, and 24.1 m/s, respectively, as simulated by ADVISOR. The power allocation performance results of the proposed strategy for the first cycle of the UDDS, SC03, and HWFET driving cycles are illustrated in Fig. 13. As seen, the peak power demand requirement of the vehicle is effectively absorbed by the SC throughout the entire driving cycle and as a result, minimizes the stress on the battery and maximizes the battery lifetime. Moreover, the SC power output staggers between positive and negative values by following the charging (regeneration) and discharging (propulsion) operations of the vehicle. As such, it effectively handles all the demand fluctuations and gives a great response capability to all the load changes of the vehicle.

2) RANDOMIZED DRIVING CYCLE

The P_{min} and v_{min} values of the randomized driving cycle as simulated in ADVISOR were obtained as 26.4 kW and

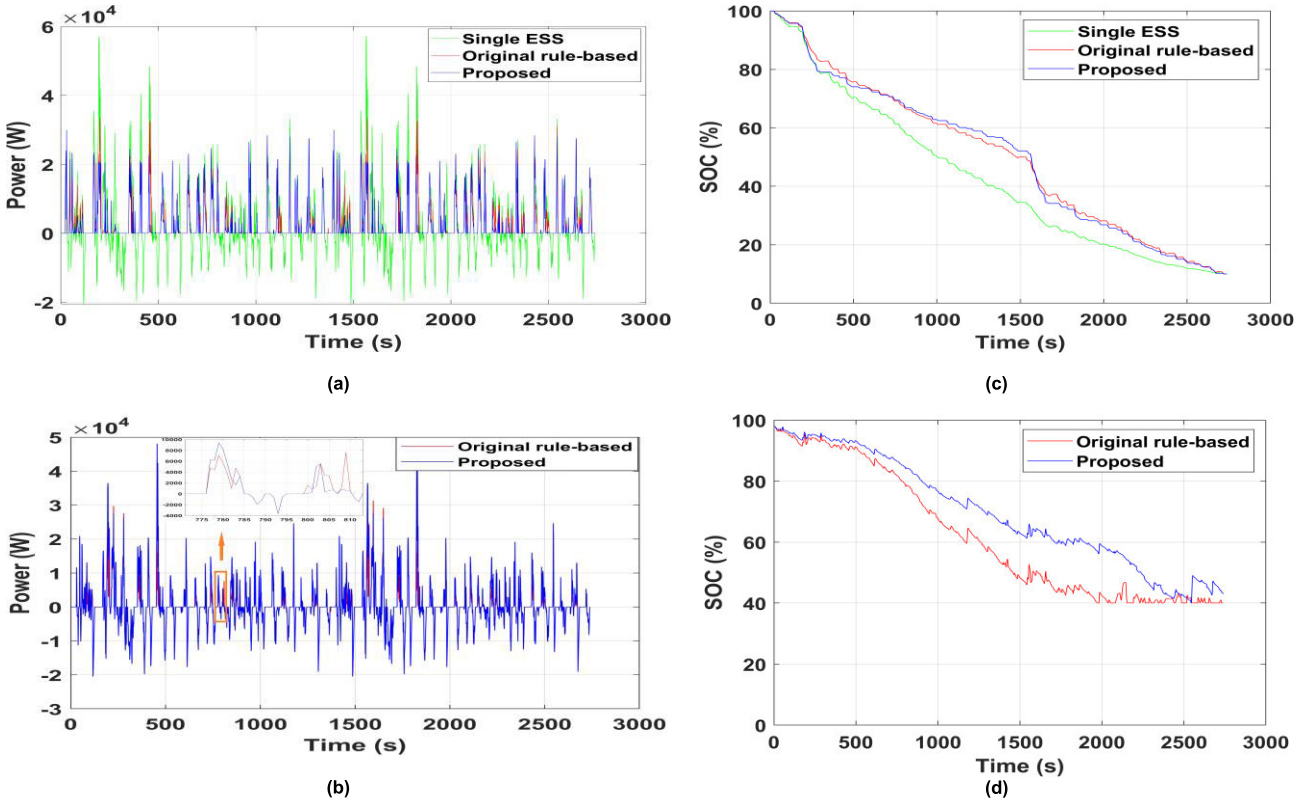

FIGURE 14. Results plot of (a) battery output power, (b) SC output power, (c) battery SOC, and (d) SC SOC for UDDS drive cycle.

TABLE 5. Performance comparison results on UDDS drive cycle.

		Battery peak propulsion power (kW)	SC peak propulsion power (kW)	Battery energy throughput (kWh)	SC energy throughput (kWh)	Battery energy loss (kWh)	SC energy loss (kWh)	Total energy loss (kWh)	Total energy (kWh)
Single ESS	Value	57.010	0.000	3.464	0.000	0.137	0.000	0.137	3.294
Original Rule-Based	Value	33.456	36.500	2.410	0.966	0.103	0.023	0.126	3.677
	%	-41.32	NA	-30.43	NA	-24.82	NA	-8.03	11.62
Proposed	Value	29.949	48.097	2.058	1.054	0.083	0.013	0.096	3.625
	%	**-47.47**	NA	**-40.59**	NA	**-39.42**	NA	**-29.92**	**10.05**

21.9 m/s respectively. The performance result of the power allocation of the proposed strategy for the first cycle of the randomized driving cycle, as shown in Fig. 13 (d) indicates that despite the degree of uncertainties and disturbances encountered while driving in unknown scenarios, the stress on the battery is effectively minimized through the absorption of the vehicle peak power demand by the SC. This ensures that the battery lifetime is maximized and the vehicle load demand fluctuations as a result of uncertainties are adequately handled.

C. COMPARATIVE ASSESSMENT

To effectively illustrate and evaluate the performance of the proposed strategy in fulfilling the overall objectives of the paper, which is to extend the battery lifetime and enhance efficiency, two other approaches are compared. The first is the single ESS where the vehicle is powered only by battery, which is also the base case and the second is the original rule-based EMS described earlier. To assess the performance of these approaches in meeting the objectives of the paper, the following evaluation parameters were considered: i) peak propulsion power, ii) energy throughput, and iii) power losses. The energy throughput is determined based on the expression [42]:

$$ET = \sum_{i=1}^{n} \frac{(C_{nom} \cdot DoD_i) \cdot C_F}{n} \tag{8}$$

where C_{nom} denotes nominal capacity, DoD_i denotes depth of discharge, and C_F denotes the number of cycles to failure for the specific DoD.

It is worth noting that to manage the energy throughput of the battery and SC, the SOCs of the battery and SC

TABLE 6. Performance comparison results on SC03 drive cycle.

		Battery peak propulsion power (kW)	SC peak propulsion power (kW)	Battery energy throughput (kWh)	SC energy throughput (kWh)	Battery energy loss (kWh)	SC energy loss (kWh)	Total energy loss (kWh)	Total energy (kWh)
Single ESS	Value	61.382	0.000	2.708	0.000	0.089	0.000	0.089	2.316
Original Rule-Based	Value	52.237	36.830	2.472	0.894	0.082	0.014	0.096	2.506
	%	-14.90	NA	-8.71	NA	-7.87	NA	7.87	8.20
Proposed	Value	39.659	39.998	2.431	1.001	0.063	0.010	0.073	2.483
	%	**-35.39**	NA	**-10.23**	NA	**-29.21**	NA	**-17.98**	**7.21**

TABLE 7. Performance comparison results on HWFET drive cycle.

		Battery peak propulsion power (kW)	SC peak propulsion power (kW)	Battery energy throughput (kWh)	SC energy throughput (kWh)	Battery energy loss (kWh)	SC energy loss (kWh)	Total energy loss (kWh)	Total energy (kWh)
Single ESS	Value	44.854	0.000	1.914	0.000	0.069	0.000	0.069	1.427
Original Rule-Based	Value	31.398	40.039	1.416	0.528	0.055	0.013	0.068	1.579
	%	-30.00	NA	-26.02	NA	-20.29	NA	-1.45	10.65
Proposed	Value	29.774	44.753	1.345	0.607	0.049	0.007	0.056	1.521
	%	**-33.62**	NA	**-29.73**	NA	**-28.99**	NA	**-18.84**	**6.59**

are used as prime indicators as they are important factors influencing battery life and the overall power loss. The power losses associated with the battery and SC during charging and discharging are determined using these expressions [31]:

$$P_{B,loss,ch} = \eta_B^2 I_B^2 R_{ch,B} - IV\,(1-\eta_B) \tag{9}$$

$$P_{B,loss,dch} = I_B^2 R_{dch,B} \tag{10}$$

$$P_{SC,loss,ch} = \eta_{SC}^2 I_{SC}^2 R_{ch,SC} - I_{SC} V\,(1-\eta_{SC}) \tag{11}$$

$$P_{SC,loss,dch} = I_{SC}^2 R_{dch,SC} \tag{12}$$

1) NON-RANDOMIZED DRIVING CYCLE

The results of the single ESS, original rule-based, and proposed approaches under the UDDS driving cycle are shown and compared in Fig. 14. Table 5 lists the performance comparisons of the three approaches under the UDDS driving cycle. The percentages represent the performance of the other approaches relative to the single ESS approach, where negative values indicate a reduction and better performance over the single ESS approach. The power output profile of the battery is shown in Fig. 14 (a). It is important to note that the battery in the single ESS (base case) has both propulsion and regenerative power as there is no SC in this case. From Fig. 14 (a), it can be observed that the original rule-based approach reduced the battery peak propulsion power from 57 kW of the single ESS approach to 33.5 kW representing a 41.32% reduction, whereas, the proposed approach further reduced it to 29.9 kW representing a 47.47% reduction compared to the base case. This reduction resulted in better utilization of the SC as its peak propulsion power increased from 36.5 kW for the original rule-based approach to 48.1 kW for the proposed approach, indicating a 31.77% increase, as shown in Fig. 14 (b). This demonstrates that the proposed approach can effectively suppress battery peak current as well as reduce battery current variation and as such extend the battery lifetime.

The SOC profiles of the battery are shown in Fig. 14 (c). As observed, the single ESS with no SC noticeably has the highest decay rate as it is the only main energy source in comparison to the other approaches. The SC SOC profiles are displayed in Fig. 14 (d). For the original rule-based approach, the SC is depleted at about 1.5 cycles while the proposed approach sustains the SC even beyond 2 cycles. This result indicates the capability of the proposed approach to ensure the availability of the SC throughout the battery discharge period, as such the battery and SC SOCs decay at an approximately similar rate. This will also give rise to better utilization of both ESS. The merits of the proposed approach can be further substantiated by the battery energy throughput (ET) results as given in Table 5. As shown in Table 5, the original rule-based approach reduced the battery ET by 30.43% in comparison to the single ESS, while the proposed approach yields a 40.59% reduction in comparison to the single ESS case. This shows that the proposed approach enhances the battery ET by approximately 15% when compared to the original rule-based approach. Correspondingly, the SC ET results as shown in Table 5 indicate that the proposed approach is the highest of the other methods, with an SC ET value of 1.054 kWh. A look at the total energy losses as seen in Table 5 indicate that in comparison to the single ESS approach, the original rule-based approach enhances the overall energy loss by 8.03%, while the proposed approach significantly enhances it by 29.92%.

Correspondingly, similar results were obtained with a further comparative assessment of the performances of the three approaches under the SC03 and HWFET driving cycles. The result for the SC03 driving cycle is provided in Table 6 while that of the HWFET driving cycle is provided in Table 7.

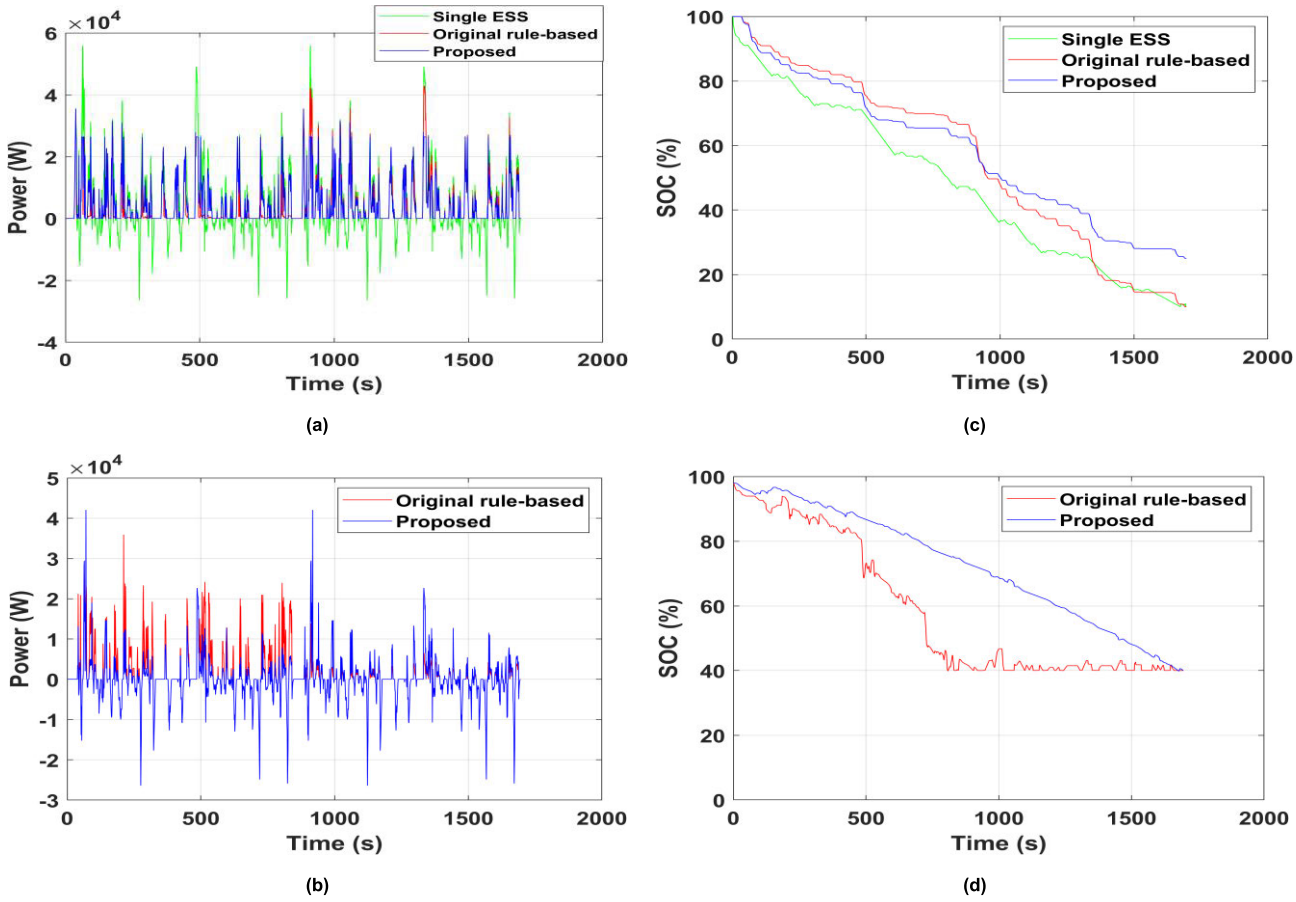

FIGURE 15. Results plot of (a) battery output power, (b) SC output power, (c) battery SOC, and (d) SC SOC for Randomized drive cycle.

TABLE 8. Performance comparison results on Randomized drive cycle.

		Battery peak propulsion power (kW)	SC peak propulsion power (kW)	Battery energy throughput (kWh)	SC energy throughput (kWh)	Battery energy loss (kWh)	SC energy loss (kWh)	Total energy loss (kWh)	Total energy (kWh)
Single ESS	Value	55.869	0.000	2.203	0.000	0.097	0.000	0.097	1.884
Original Rule-Based	Value	42.918	35.918	1.911	0.713	0.080	0.015	0.095	2.075
	%	-23.18	NA	-13.25	NA	-17.53	NA	-2.06	10.13
Proposed	Value	35.563	42.054	1.725	0.818	0.065	0.009	0.074	2.034
	%	**-36.35**	NA	**-21.70**	NA	**-32.99**	NA	**-23.71**	**7.96**

The proposed approach outperformed the other approaches regardless of the driving cycle. The SC energy is effectively utilized not just for one drive cycle, but for the entire battery discharge period (i.e., multiple cycles).

2) RANDOMIZED DRIVING CYCLE

The results of the single ESS, original rule-based, and proposed approaches for the randomized driving cycle are provided in Fig. 15 and Table 8. Similar to the non-randomized driving cycles and as shown in Fig. 15 (a), the battery peak propulsion power was reduced from 55.9 kW of the single ESS approach to 42.9 kW of the original rule-based approach. This result depicts a 23.18% reduction. However, the proposed approach reduced it to 35.6 kW, depicting a 36.35% reduction in comparison with the single ESS. Correspondingly, the SC peak propulsion power as shown in Fig. 15 (b), rose from 35.9 kW of the original rule-based to 42.1 kW of the proposed approach depicting an increment of 17.08%. These results indicate better utilization of the SC and reduced battery current variation despite the huge fluctuations in load demand caused by the uncertainties of the unknown driving scenario.

The battery SOC profiles as shown in Fig. 15 (c) reveal that while the single ESS had the highest decay rate, the original rule-based approach had the least decay rate in the first cycle.

This implies a corresponding highest SC decay rate for the first cycle, as shown in the SC SOC profile in Fig. 15 (d). However, this could not be sustained in the second cycle as the battery in the original rule-based approach decayed faster in the second cycle when compared to the proposed approach. As observed, the faster decay rate of the battery of the original rule-based approach in the second cycle was obviously in meeting the vehicle power demands as the SC could not support much during this period, having reached its minimum level. This reveals the intelligence brought about by the ANN in the proposed approach which considers the vehicle velocity, the current status of the SC, and the battery SOC before determining how much power the SC should support the propulsion with at periods when $P_{Req} \leq P_{min}$. Hence, for the original rule-based approach, SC is depleted after one cycle, whereas the proposed approach sustains the SC throughout the battery discharge period (i.e., 2 cycles). Furthermore, the battery ET results displayed in Table 8 show that in comparison to the single ESS, the original rule-based approach and the proposed approach reduced the battery ET by 13.25% and 21.70% respectively. This result shows that the proposed approach enhances the battery ET by 9.73% in comparison to the original rule-based approach. Also, the proposed approach had the highest SC ET of about 0.818 kWh.

Evaluating how well each approach was able to reduce energy losses in comparison to the single ESS reveals that the original rule-based approach enhances the overall energy loss by 2.06%, while the proposed approach enhances it significantly by 23.71%. Furthermore, the sum total of all the energy losses for the original rule-based approach under the UDDS, SC03, HWFET, and randomized drive cycles, as shown in Tables 5-8, gives 0.385 kWh while that of the proposed strategy gives 0.299 kWh. This represents approximately a 22.5% reduction in the total energy loss. Based on the obtained results, it can be inferred that in comparison to the other approaches, the proposed approach can effectively enhance the overall energy efficiency, reduce battery energy throughput and improve battery lifetime.

VI. CONCLUSION

In this paper, an adaptive velocity predictor based on an LSTM network and an artificial neural network enhanced energy management strategy that aims at better utilization of the two energy sources of a battery-supercapacitor hybrid electric vehicle was proposed. First, feature engineering was utilized to extend the features of the original driving cycle dataset of the known driving condition scenarios. The LSTM network used for the vehicle future velocity prediction of the unknown driving condition scenario utilized a multiple time-series prediction scheme. The results showed that, for each of the non-randomized (i.e. UDDS, SC03, and HWFET) and randomized test driving cycles used, the scheme when compared with the other prediction schemes, improved the velocity prediction accuracy by at least 45.98%. This result implies that the velocity predictor model can learn driving conditions of known scenarios, adaptively adjust and predict future velocity in real-time when encountering unknown driving conditions. Next, to distribute the vehicle power demand amongst the battery and SC, an original rule-based EMS was proposed. However, to manage the energy losses, ensure the availability of the SC throughout the battery discharge period, and achieve better utilization of the battery and SC, an artificial neural network-based approach was designed and incorporated into the rules. Simulation results showed that the proposed approach in comparison to the single ESS (battery alone) and the original rule-based approaches, reduced battery peak propulsion power by at least 33.62% across the four driving cycles. Thus, ensures efficient utilization of the SC energy throughout the complete battery discharge period (i.e., multiple cycles). Furthermore, the results shown in the paper indicate that for each of the four driving cycles, the proposed approach in comparison with other methods, enhanced battery energy throughput and the overall total energy loss by at least 10.23% and 17.98% respectively. These improvements reflect the effectiveness of the proposed approach to prolong battery lifetime and enhance efficiency.

REFERENCES

[1] B. Li, M. Chen, Z. Ma, G. He, W. Dai, D. Liu, C. Zhang, and H. Zhong, "Modeling integrated power and transportation systems: Impacts of power-to-gas on the deep decarbonization," *IEEE Trans. Ind. Appl.*, vol. 58, no. 2, pp. 2677–2693, Mar. 2022.

[2] Y. Yang, Y. Xu, H. Zhang, F. Yang, J. Ren, X. Wang, P. Jin, and D. Huang, "Research on the energy management strategy of extended range electric vehicles based on a hybrid energy storage system," *Energy Rep.*, vol. 8, pp. 6602–6623, Nov. 2022.

[3] L. Zhang, X. Ye, X. Xia, and F. Barzegar, "A real-time energy management and speed controller for an electric vehicle powered by a hybrid energy storage system," *IEEE Trans. Ind. Informat.*, vol. 16, no. 10, pp. 6272–6280, Oct. 2020.

[4] L. Kouchachvili, W. Yaïci, and E. Entchev, "Hybrid battery/supercapacitor energy storage system for the electric vehicles," *J. Power Sources*, vol. 374, pp. 237–248, Jan. 2018.

[5] E. Naderi, M. Ansari, and A. Asrari, "Experimental validation of a hybrid storage framework to cope with fluctuating power of hybrid renewable energy-based systems," *IEEE Trans. Energy Convers.*, vol. 36, no. 3, pp. 1991–2001, Sep. 2021.

[6] J. Chen, L. Qian, and L. Xuan, "Cooperative control of connected hybrid electric vehicles and traffic signals at isolated intersections," *IET Intell. Transp. Syst.*, vol. 14, no. 13, pp. 1903–1912, Dec. 2020.

[7] F. Xu, X. Jiao, Y. Wang, and Y. Jing, "Battery-lifetime-conscious energy management strategy based on SP-SDP for commuter plug-in hybrid electric vehicles," *IEEJ Trans. Electr. Electron. Eng.*, vol. 13, no. 3, pp. 472–479, Mar. 2018.

[8] J. Armenta, C. Núñez, N. Visairo, and I. Lázaro, "An advanced energy management system for controlling the ultracapacitor discharge and improving the electric vehicle range," *J. Power Sources*, vol. 284, pp. 452–458, Jun. 2015.

[9] Y. Shen, Y. Li, Y. Tang, J. Sun, J. Zhao, and X. Yang, "An energy management strategy based on fuzzy logic for hybrid energy storage system in electric vehicles," *IEEJ Trans. Electr. Electron. Eng.*, vol. 17, no. 1, pp. 53–60, Jan. 2022.

[10] X. Wang, H. He, F. Sun, and J. Zhang, "Application study on the dynamic programming algorithm for energy management of plug-in hybrid electric vehicles," *Energies*, vol. 8, no. 4, pp. 3225–3244, Apr. 2015.

[11] C. Zheng, W. Li, and Q. Liang, "An energy management strategy of hybrid energy storage systems for electric vehicle applications," *IEEE Trans. Sustain. Energy*, vol. 9, no. 4, pp. 1880–1888, Oct. 2018.

[12] N. Kim, S. Cha, and H. Peng, "Optimal control of hybrid electric vehicles based on Pontryagin's minimum principle," *IEEE Trans. Control Syst. Technol.*, vol. 19, no. 5, pp. 1279–1287, Sep. 2011.

[13] A. Santucci, A. Sorniotti, and C. Lekakou, "Power split strategies for hybrid energy storage systems for vehicular applications," *J. Power Sources*, vol. 258, pp. 395–407, Jul. 2014.
[14] K. Wang, W. Wang, L. Wang, and L. Li, "An improved SOC control strategy for electric vehicle hybrid energy storage systems," *Energies*, vol. 13, no. 20, p. 5297, Oct. 2020.
[15] V. Sezer, M. Gokasan, and S. Bogosyan, "A novel ECMS and combined cost map approach for high-efficiency series hybrid electric vehicles," *IEEE Trans. Veh. Technol.*, vol. 60, no. 8, pp. 3557–3570, Oct. 2011.
[16] M. Sellali, A. Betka, A. Djerdir, Y. Yang, I. Bahri, and S. Drid, "A novel energy management strategy in electric vehicle based on H_∞ self-gain scheduled for linear parameter varying systems," *IEEE Trans. Energy Convers.*, vol. 36, no. 2, pp. 767–778, Jun. 2021.
[17] G. Buccoliero, P. G. Anselma, S. A. Bonab, G. Belingardi, and A. Emadi, "A new energy management strategy for multimode power-split hybrid electric vehicles," *IEEE Trans. Veh. Technol.*, vol. 69, no. 1, pp. 172–181, Jan. 2020.
[18] A. Florescu, A. I. Bratcu, I. Munteanu, A. Rumeau, and S. Bacha, "LQG optimal control applied to on-board energy management system of all-electric vehicles," *IEEE Trans. Control Syst. Technol.*, vol. 23, no. 4, pp. 1427–1439, Jul. 2015.
[19] M. Masih-Tehrani, M. R. H. Yazdi, V. Esfahanian, M. Dahmardeh, and H. Nehzati, "Wavelet-based power management for hybrid energy storage system," *J. Mod. Power Syst. Clean Energy*, vol. 7, no. 4, pp. 779–790, Jul. 2019.
[20] L. Qiu, L. Qian, H. Zomorodi, and P. Pisu, "Global optimal energy management control strategies for connected four-wheel-drive hybrid electric vehicles," *IET Intell. Transp. Syst.*, vol. 11, no. 5, pp. 264–272, Jun. 2017.
[21] S. Onori, L. Serrao, and G. Rizzoni, *Hybrid Electric Vehicles: Energy Management Strategies*. Heidelberg, Germany: Springer, 2016.
[22] Z. Chen, R. Xiong, C. Wang, and J. Cao, "An on-line predictive energy management strategy for plug-in hybrid electric vehicles to counter the uncertain prediction of the driving cycle," *Appl. Energy*, vol. 185, pp. 1663–1672, Jan. 2017.
[23] S. Xie, X. Hu, S. Qi, and K. Lang, "An artificial neural network-enhanced energy management strategy for plug-in hybrid electric vehicles," *Energy*, vol. 163, pp. 837–848, Nov. 2018.
[24] Z. Chen, C. C. Mi, J. Xu, X. Gong, and C. You, "Energy management for a power-split plug-in hybrid electric vehicle based on dynamic programming and neural networks," *IEEE Trans. Veh. Technol.*, vol. 63, no. 4, pp. 1567–1580, May 2013.
[25] Q. Zhang, L. Wang, G. Li, and Y. Liu, "A real-time energy management control strategy for battery and supercapacitor hybrid energy storage systems of pure electric vehicles," *J. Energy Storage*, vol. 31, Oct. 2020, Art. no. 101721.
[26] T. Liu, X. Tang, H. Wang, H. Yu, and X. Hu, "Adaptive hierarchical energy management design for a plug-in hybrid electric vehicle," *IEEE Trans. Veh. Technol.*, vol. 68, no. 12, pp. 11513–11522, Jul. 2019.
[27] H. Guo, F. Zhao, H. Guo, Q. Cui, E. Du, and K. Zhang, "Self-learning energy management for plug-in hybrid electric bus considering expert experience and generalization performance," *Int. J. Energy Res.*, vol. 44, no. 7, pp. 5659–5674, Jun. 2020.
[28] K. Vatanparvar, S. Faezi, I. Burago, M. Levorato, and M. A. A. Faruque, "Extended range electric vehicle with driving behavior estimation in energy management," *IEEE Trans. Smart Grid*, vol. 10, no. 3, pp. 2959–2968, May 2019.
[29] R. Carter, A. Cruden, and P. J. Hall, "Optimizing for efficiency or battery life in a battery/supercapacitor electric vehicle," *IEEE Trans. Veh. Technol.*, vol. 61, no. 4, pp. 1526–1533, May 2012.
[30] T. Markel, A. Brooker, T. Hendricks, V. Johnson, K. Kelly, B. Kramer, M. O'Keefe, S. Sprik, and K. Wipke, "Advisor: A systems analysis tool for advanced vehicle modeling," *J. Power Sources*, vol. 110, no. 2, pp. 255–266, 2002.
[31] (2013). *ADVISOR Advanced Vehicle Simulator*. [Online]. Available: http://adv-vehicle-sim.sourceforge.net
[32] K. Alobeidli and V. Khadkikar, "A new ultracapacitor state of charge control concept to enhance battery lifespan of dual storage electric vehicles," *IEEE Trans. Veh. Technol.*, vol. 67, no. 11, pp. 10470–10481, Nov. 2018.
[33] C. Sun, X. Hu, S. J. Moura, and F. Sun, "Velocity predictors for predictive energy management in hybrid electric vehicles," *IEEE Trans. Control Syst. Technol.*, vol. 23, no. 3, pp. 1197–1204, May 2015.
[34] D. Shah, W. Campbell, and F. H. Zulkernine, "A comparative study of LSTM and DNN for stock market forecasting," in *Proc. IEEE Int. Conf. Big Data (Big Data)*, Dec. 2018, pp. 4148–4155.
[35] C. Udeogu, A. Caliwag, and W. Lim, "Remaining useful life prediction for supercapacitors using an optimized end-to-end deep learning approach," *J. Korean Inst. Commun. Inf. Sci.*, vol. 47, no. 3, pp. 482–491, Mar. 2022.
[36] M. Udurume, C. Udeogu, A. Caliwag, and W. Lim, "Synthetic data generation using GAN for RUL prediction of supercapacitors," *J. Korean Inst. Commun. Inf. Sci.*, vol. 47, no. 3, pp. 492–500, Mar. 2022.
[37] R. Wang and S. M. Lukic, "Review of driving conditions prediction and driving style recognition based control algorithms for hybrid electric vehicles," in *Proc. IEEE Vehicle Power Propuls. Conf.*, Sep. 2011, pp. 1–7.
[38] K. Han, Y. Yu, D. Na, H. Jung, Y. Heo, H. Jeong, S. Yun, and J. Kim, "Understanding postal delivery areas in the republic of Korea using multiple unsupervised learning approaches," *ETRI J.*, vol. 44, no. 2, pp. 232–243, Apr. 2022.
[39] T. Wang, Q. Li, D. J. Bucci, Y. Liang, B. Chen, and P. K. Varshney, "K-medoids clustering of data sequences with composite distributions," *IEEE Trans. Signal Process.*, vol. 67, no. 8, pp. 2093–2106, Apr. 2019.
[40] A. Ng, *CS229 Course Notes: Deep Learning*. Stanford, CA, USA: Stanford Univ., 2018.
[41] T. K. Chau, S. S. Yu, T. Fernando, H. H.-C. Iu, and M. Small, "A load-forecasting-based adaptive parameter optimization strategy of STATCOM using ANNs for enhancement of LFOD in power systems," *IEEE Trans. Ind. Informat.*, vol. 14, no. 6, pp. 2463–2472, Jun. 2018.
[42] H. Bindner, T. Cronin, P. Lundsager, J. Manwell, U. Abdulwahid, and I. Baring-Gould, "Lifetime modelling of lead acid batteries," Dept. Inf. Service, Riso Nat. Lab., Roskilde, Denmark, Tech. Rep. Ris0-R-1515, 2005.

CHIGOZIE UZOCHUKWU UDEOGU (Student Member, IEEE) received the B.Eng. degree in electrical electronics engineering from the Federal University of Technology, Owerri, Nigeria, in 2013. He is currently pursuing the M.Sc. degree in electronics engineering with the Kumoh National Institute of Technology (KIT), Gumi, South Korea. He has been a Research Assistant with the Future Communications and Systems Laboratory, KIT, since 2021. His research interests include but not limited to energy management systems, machine learning, data analysis, and electric vehicles.

WANSU LIM (Member, IEEE) received the Ph.D. degree from the Gwangju Institute of Science and Technology (GIST), South Korea, in 2010. He is currently an Associate Professor with the Kumoh National Institute of Technology, South Korea. From 2010 to 2014, he was a Research Fellow (2010–2013) at the University of Hertfordshire, U.K., and then a Postdoctoral Researcher (2013–2014) at the Institut National de la Recherche Scientifique (INRS), Montreal, Canada. His research interests include statistical analysis, machine learning, and optimization.